CHEMISTRY OF MATERIALS
Cite This: Chem. Mater. 2020, 32, 468−475
Article
pubs.acs.org/cm

Electrochromic Niobium Oxide Nanorods

Gary K. Ong,[†,∥] Camila A. Saez Cabezas,[†,∥] Manuel N. Dominguez,[†,‡] Susanne Linn Skjærvø,[†,§] Sungyeon Heo,[†] and Delia J. Milliron*[,†]

[†]McKetta Department of Chemical Engineering, The University of Texas at Austin, 200 East Dean Keeton Street, Austin, Texas 78712, United States

[‡]Department of Chemistry, The University of Texas at Austin, 105 East 24th Street, Austin, Texas 78712, United States

[§]Department of Chemistry and Nanoscience Center, University of Copenhagen, 2100 København Ø, Denmark

Supporting Information

ABSTRACT: Niobium oxide (Nb_2O_5) is an interesting active material for technologies ranging from catalysis and sensors to energy storage and electrochromic devices owing to its unique optical, electronic, and electrochemical properties. These properties vary between different phases and morphologies in the Nb_2O_5 system, but systematic studies that correlate properties to phase and morphology are limited by current synthetic methods, which require postsynthetic high temperature treatments and suffer from a lack of direct and precise control over morphology, crystal structure, and stoichiometry. Here, we report a heat-up colloidal synthesis method that produces orthorhombic Nb_2O_5 nanorods 1 nm in width by 31 nm in length that preferentially grow along the [001] direction. The synthesis is based on aminolysis of niobium oleate in octadecene, and nanorods are formed through three distinct steps: aminolysis-driven formation of niobium oxo clusters, condensation into amorphous Nb_2O_5 seeds below the reaction temperature (240 °C, under atmospheric pressure), and crystallization and growth of Nb_2O_5 nanorods. We investigated the electrochromic behavior of nanorod thin films upon Li^+ intercalation and observed predominantly near-infrared coloration, fast switching kinetics, and durability for at least 500 charge−discharge cycles.

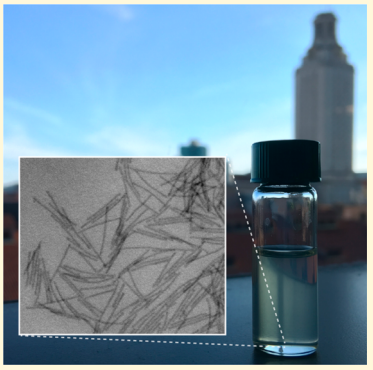

INTRODUCTION

Niobium oxide has garnered significant interest in the recent decade as an active material in applications ranging from electrochemical devices such as batteries[1,2] and electrochromic windows[3−7] to solar devices[8−10] and chemical sensors.[11−13] The development of these technologies is enabled by the unique combination of optical, electronic, and electrochemical properties of niobium oxide such as a wide band gap, high dielectric constant, medium to high refractive index, and fast Li^+ transport.[14,15] As an electrochromic material, niobium oxide is one of the oldest known, having been studied for about as long as tungsten oxide. The coloration is attributed to the intercalation of Li^+ into the niobium oxide lattice accompanied by the reduction of niobium oxide expressed in the following formula:

$$Nb_2O_5 + xLi^+ = Li_xNb_2O_5 \quad (1)$$

While the intercalative mechanism remains the same, the electrochromic properties of the various phases of niobium oxide and their amorphous counterpart vary significantly. The first observable distinction is a difference in coloration upon Li^+ intercalation: brown for amorphous niobium oxide and blue for crystalline niobium oxide. Work by Fu et al. provides insight into this phenomenon: amorphous niobium oxide absorbs with two distinct bands at 440 and 620 nm while crystalline niobium oxide absorbs with just one absorption band at 700 nm.[3] These observations are further supported by Schmitt and co-workers with an additional caveat that the observable coloration transitions from the visible to the near-infrared when the crystallite size exceeds 30 nm.[16] Beyond coloration, key electrochromic parameters such as the magnitude of optical modulation, coloration efficiency, durability, and kinetics also differ between crystalline and amorphous niobium oxide: it was found that crystalline niobium oxide switches faster, and is more durable than amorphous niobium oxide.[3,17−19]

Systematic study of these phenomena for the niobium oxide system is impeded by the incongruence between typical heat-up synthetic protocols and the complex niobium oxide phase diagram.[20,21] Prior work on the synthesis of crystalline niobium oxides has focused principally on hydrothermal approaches[22−29] that yield niobium oxides of various shapes and dimensionality. Yet, they have not been investigated in electrochromic applications, likely due to their colloidal instability preventing the deposition of optical quality films. In contrast, studies on niobium oxide electrochromic properties have used solid-state deposition[17,30,31] or sol−gel[16,32] processed thin films. In the former, shape and dimensionality

Received: October 3, 2019
Revised: December 20, 2019
Published: December 31, 2019

DOI: 10.1021/acs.chemmater.9b04061
Chem. Mater. 2020, 32, 468−475

are difficult to control, while in the latter, high crystal quality and phase purity can be difficult to realize.

Colloidal nanocrystal synthesis is an effective way to impose strict dimensional and phase control on materials and has been applied extensively to a variety of nanocrystal systems including metal nanoparticles,[33] metal oxides[34−36] and doped metal oxides, and metal chalcogenides.[37] Specific to the niobium oxide system, one report by Jana and Rioux showed the synthesis of niobium oxide nanobars and nanoplatelets with Raman and X-ray diffraction that suggests the tetragonal Nb_2O_5 and NbO_2 crystal structures using seeded growth and high temperature thermal decomposition of niobium oleate.[38] That work was an important first step toward the development of colloidal synthesis methods that yield size controlled and phase pure niobium oxide materials. However, a mechanistic understanding of the synthetic process was not elucidated, and the influence of nanostructuring through colloidal synthesis on the resulting properties compared to bulk niobium oxide systems remains to be investigated.

Building on the aforementioned progress on the colloidal synthesis of niobium oxide, we present a mechanistic study of the synthesis of niobium oxide nanorods that is derived from the aminolysis of niobium oleate and demonstrate the utility of the nanorods as an electrochromic material. The synthesis was developed to promote nanorod formation at significantly lower temperatures to sidestep agglomeration difficulties present in prior syntheses, which was carried out at higher temperatures above 270 °C, thus enabling the solution-based processing of these nanorods into optical quality thin films. Using a combination of microscopy, X-ray diffraction, and infrared, nuclear magnetic resonance, and Raman spectroscopy analyses, we elucidate the mechanism underlying the nanorod formation that starts with the in situ formation of a chloro oleyl niobium(V) complex followed by the formation of amorphous niobium oxide seeds that then crystallize into orthorhombic niobium oxide (T-Nb_2O_5) nanorods. Then, we investigate the electrochromic properties of nanorod thin films and discuss core electrochromic characteristics such as their coloration behavior, cyclic stability, and kinetics. Unlike prior reports on the electrochromism of niobium oxides that are centered on electrochromic modulation in the visible regime, these films exhibit electrochromism that is predominantly in the infrared with a significantly diminished visible electrochromic response. This difference is attributed to the dimensional constraint of the nanorod shape in the radial direction inhibiting the inherent polaronic coloration of Nb_2O_5 in the visible regime while maintaining the infrared polaronic response.

EXPERIMENTAL SECTION

Materials. All chemicals were used as received and without further purification. Niobium chloride ($NbCl_5$, 99%), oleic acid (technical grade, 90%), 1-octadecene (technical grade, 90%), *N*,*N*-dimethylformamide (ACS reagent, ≥99.8%), nitrosonium tetraborofluorate (95%), acetonitrile (ACS reagent, ≥99.5%), tetraethylene glycol dimethyl ether (tetraglyme, ≥99%), and tetrabutylammonium bis-trifluoromethanesulfonimidate (TBATFSI, >99.0%) were purchased from Sigma-Aldrich. Oleylamine (C-18 content 80−90%) was purchased from Acros Organics. Toluene (≥99.5%) and hexane (ACS reagent, various methylpentanes 4.2%, ≥98.5%) were purchased from Fisher Scientific. Lithium bis-(trifluoromethanesulfonyl)imide (LiTFSI, 3M Fluorad) was purchased from 3M.

Nanorod Synthesis. The synthesis of T-Nb_2O_5 nanorods is based on established colloidal synthesis methods. The reaction mixture was prepared in a nitrogen glovebox and kept in an air-free environment while it was transferred to the Schlenk line. Briefly, 0.545 g (2 mmol) of $NbCl_5$ was mixed with 3.127 g (11 mmol) of oleic acid and 10 g (40 mmol) of octadecene. The reagents were stirred at room temperature under nitrogen until $NbCl_5$ was fully dissolved and a blood red solution of chloro oleyl niobium(V) was formed. This solution was degassed at 120 °C for 30 min. Then, a mixture of oleylamine (0.534 g or 2 mmol) and octadecene (0.789 g) was injected into the reaction flask at 120 °C under nitrogen. After the injection, the solution was degassed at 120 °C for 15 min, heated to 240 °C, and allowed to react for 30 min under nitrogen. Once the solution cooled to 70 °C, 7.5 mL of toluene was injected into the flask to dilute the mixture. The nanorods were recovered and purified by precipitating with isopropanol, centrifuging at 3500 rpm for 10 min, and redispersing in toluene. Precipitation and redispersion were repeated two more times.

Ligand Stripping. The native organic ligands on the nanorod surface were stripped following a previously established method.[39] In a typical procedure, 5 mg of nitrosonium tetrafluoroborate was added to a mixture containing 1 mL of a 5 mg/mL nanorod dispersion and 1 mL of *N*,*N*-dimethylformamide (DMF). This solution was sonicated for 30 min and then left to settle to allow the nanorods to precipitate. The nanorods were then dispersed in 1 mL of DMF. This dispersion was mixed with an equal volume of hexane, shaken, and left to settle to remove the top hexane layer. This step was repeated three times. Finally, the nanorods were purified by performing five cycles of flocculation with toluene, centrifugation at 4000 rpm for 5 min, and redispersion in DMF.

Thin Film Deposition. Ligand-stripped nanorods were dispersed in a 1:1 mixture of DMF and acetonitrile (30 mg/mL) and spin-coated at 1250 rpm on fluorine-doped tin oxide (FTO) coated glass substrates.

Electron Microscopy. Electron microscopy was performed on a Hitachi S5500 SEM/STEM instrument. Nanorods were imaged in bright-field scanning transmission electron (STEM) mode at a 30 kV accelerating voltage. Samples were drop-cast on Type-A ultrathin carbon copper TEM grids (Ted Pella, 01822, 400 mesh) from dilute nanorod dispersions in toluene. Nanorod films deposited on silicon substrates were imaged in scanning electron (SEM) mode at a 30 kV accelerating voltage.

X-ray Diffraction (XRD). Powder diffraction patterns were collected on a Rigaku R-Axis Spider using Cu Kα radiation (1.54 Å). Powders were obtained by precipitation from solution with isopropanol, centrifugation at 7000 rpm for 5 min, and drying under vacuum for 24 h. Samples were mounted on a cryoloop using mineral oil.

Raman Spectroscopy. Raman spectroscopy was performed with a Horiba LabRAM HR Evolution instrument equipped with a confocal microscope. Spectra were collected using a 532 nm laser source, 50 mW power, 50× objective, and 1 μm laser spot size. Powder samples were identical to the ones prepared for X-ray diffraction measurements. The bulk orthorhombic Nb_2O_5 powder used as a reference in Figure 5 was prepared by annealing a decaniobate ($[N(CH_3)_4]_6Nb_{10}O_{28}$) polyoxometalate powder at 600 °C for 12 h under air.[40,41]

Fourier Transform Infrared (FTIR) Spectroscopy. FTIR spectroscopy was carried out in transmission geometry with a 4 cm^{-1} resolution and an average of 128 scans on a Bruker Vertex 70 spectrometer. Chloro oleyl niobium(V) samples were transferred into a sealed liquid cell with KBr windows and a 0.0125 mm path length under inert conditions. Ligand-capped and ligand-stripped nanorod films were spin-coated on 1 × 1 cm undoped silicon substrates.

Nuclear Magnetic Resonance (NMR) Spectroscopy. NMR spectroscopy was performed on an Agilent 400 MHz instrument using a OneNMR probe with Protune accessory. The ^1H NMR was taken in a range of −2 to 14 ppm with 128 scans and a relaxation delay of 2 s with a pulse angle of 30°. The samples were prepared under an inert atmosphere and diluted into DMSO-d_6 (10 μL, 600 μL).

Spectroelectrochemical Modulation. In situ spectroelectrochemical measurements were performed using a custom-built cell in

DOI: 10.1021/acs.chemmater.9b04061
Chem. Mater. 2020, 32, 468−475

an Ar glovebox connected to a potentiostat (Biologic VMP3) and a spectrometer (ASD Quality Spec Pro). A three-electrode configuration is used in a typical experiment: Li foil (MTI) is both the counter and reference electrodes and the nanorod film on FTO-coated glass is the working electrode. The transmittance of the nanorod film immersed in LiTFSI in anhydrous tetraglyme electrolytes of varying concentration (0.1, 1, and 3 M) is recorded as a function of wavelength at each applied potential (1.2 and 4.0 V vs Li/Li^+ for charging and discharging, respectively). LiTFSI in tetraglyme was the most stable electrolyte in this voltage range compared to other Li salt and solvent combinations (Figure S1). This setup was also used to conduct cyclic voltammetry, cycling stability, and coloration efficiency experiments (see additional methods in the Supporting Information). Spectroelectrochemical experiments with the nonintercalating 1 M TBATFSI in tetraglyme electrolyte were also performed using a three-electrode configuration, but in this case, Pt foil is the counter electrode, nonaqueous Ag/Ag^+ is the reference electrode, and the nanorod film on FTO-coated glass is the working electrode.

X-ray Photoelectron Spectroscopy (XPS). XPS was carried out with a Kratos X-ray photoelectron spectrometer—AXIS Ultra DLD using an Al Kα source. Samples were identical to the nanorod films spin-coated on FTO for spectroelectrochemical modulation.

RESULTS AND DISCUSSION

To design the one-pot colloidal synthesis of niobium oxide, we began with a well-established starting point for the synthesis of many metal oxides: the decomposition of a metal carboxylate, specifically a metal oleate.[42−44] In agreement with the results of Jana and Rioux, simple thermal decomposition of the metal oleate, formed in situ through a reaction of niobium(V) chloride with oleic acid, required high temperatures exceeding 270 °C. The synthesis yielded nanorods that were, however, irreversibly aggregated (Figure S2, Supporting Information) and unsuitable for the formation of homogeneous electrochromic films. To yield a colloidally stable product, we altered the reaction mechanism to one based on aminolysis of the metal oleate complex with a primary amine. The results of the synthesis are summarized in Figure 1. As-synthesized, the nanorods are in the orthorhombic T-Nb_2O_5 phase with a significant aspect ratio of ca. 1 nm width by 31 nm length (Figure S3). The long axis of the nanorod (direction of growth) is the [001] direction as supported by the significant broadening of all peaks in the XRD pattern with the exception of planes in the {001} family. The Raman spectrum of a powder sample of this material is in general agreement with the one reported for bulk T-Nb_2O_5: it is dominated by a strong band at 685 cm^{-1} characteristic of stretching modes from niobium−oxygen bridges arranged in octahedral and pentagonal polyhedra structures. The weaker and broader bands at 250 and 800 cm^{-1} correspond to bending modes from niobium−oxygen bridges and a low concentration of terminal niobium−oxygen double bonds, respectively.[45]

To uncover the underlying synthetic mechanism, we performed an aliquot study on the reaction starting from the formation of the metal oleate complex to the final formation of the nanorods at the end of the synthesis: the results were analyzed with a combination of electron microscopy (STEM), Raman spectroscopy, XRD, NMR, and FTIR spectroscopy. True to the synthetic design, FTIR spectroscopy and NMR show formation of a metal oleate complex upon mixing of niobium(V) chloride and oleic acid in octadecene (Figure 2). However, the metal oleate complex that is formed is not a completely exchanged niobium oleate as previously suggested by Jana and Rioux. It is more accurately described as a chloro

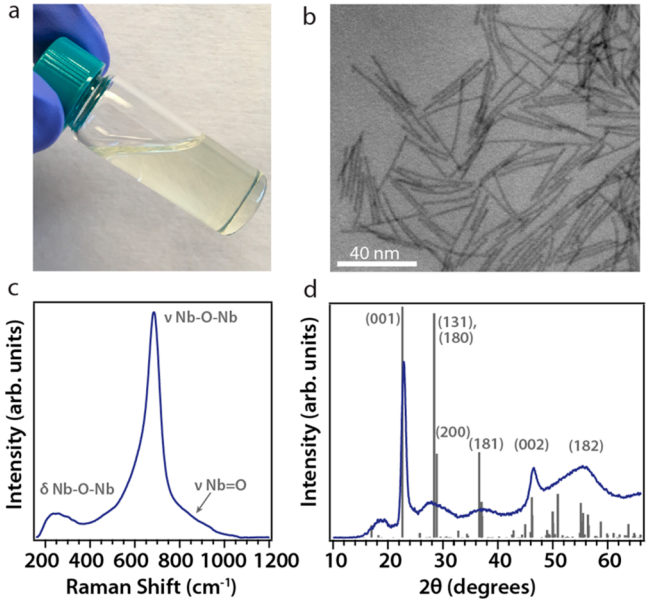

Figure 1. Characterization of T-Nb_2O_5 nanorods. (a) Photograph of the colloid dispersed in toluene, (b) STEM image of the nanorods, (c) Raman spectrum of the nanorods, and (d) powder XRD pattern of the nanorods (blue) and T-Nb_2O_5 reference (gray, PDF No. 00-027-1003).

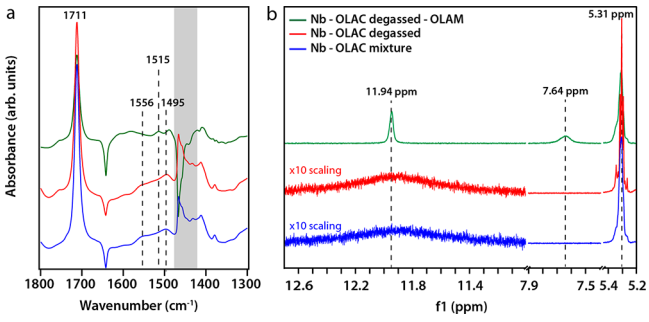

Figure 2. Characterization of niobium complex. (a) FTIR spectra of aliquots collected at initial mixing, subsequent degassing, and with addition of oleylamine. The over-subtracted peak in the shaded region of the green spectrum is due to the removal of low molecular weight hydrocarbons during degassing. (b) NMR spectra of the same aliquots.

oleyl niobium(V) complex. Our results support prior reports in literature showing that oleic acid can be deprotonated completely to form a niobium chloro complex with bridging oleates at low ratios of niobium-to-oleic acid such as a 1 to 1 ratio.[46] This is signified by the absence of the protonated carboxylic acid peak at 1711 cm^{-1} and emergence of the niobium carboxylate peaks at 1556 and 1495 cm^{-1} in FTIR spectra (Figure 2a and Figure S4), which agree with the values reported by Marchetti et al.[37] However, with increasing oleic acid in solution, the niobium carboxylate peak remains relatively constant suggesting that the exchange halts after a 1 to 3 niobium-to-oleic acid ratio. Thus, the niobium oleate that is formed is likely a chloro oleyl niobium(V) composed of two to three oleate ligands with the remaining shell satisfied by chloride species. This remains unchanged upon heating or degassing of the solution. Upon injection of oleylamine, a new peak emerges at 1515 cm^{-1} that we assign to N−H bending, suggesting formation of an amide through reaction of the

DOI: 10.1021/acs.chemmater.9b04061
Chem. Mater. 2020, 32, 468−475

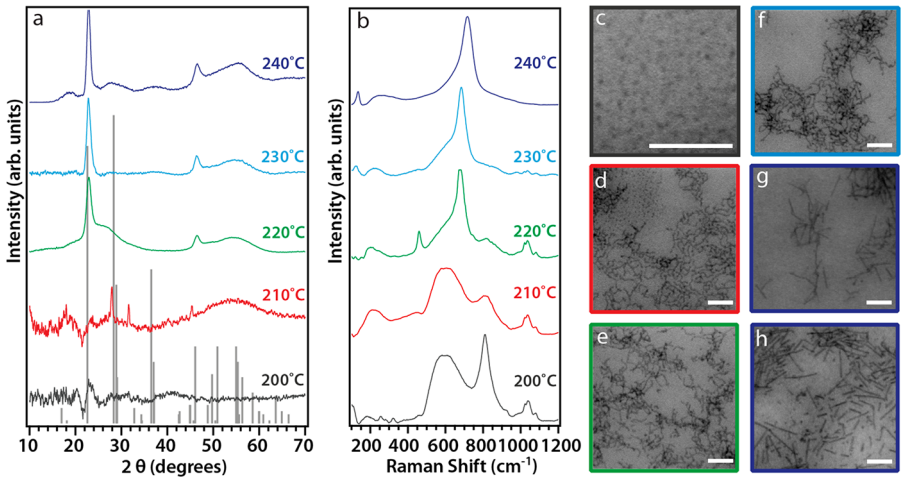

Figure 3. Characterization of temperature aliquots. (a) Powder XRD of aliquots collected from 200 to 240 °C, (b) powder Raman of aliquots collected from 200 to 240 °C, (c) STEM image of 200 °C aliquot, (d) STEM image of 210 °C aliquot, (e) STEM image of 220 °C aliquot, (f) STEM image of 230 °C aliquot, (g) STEM image of 240 °C aliquot collected at 1 min, and (h) STEM image of 240 °C aliquot collected at 15 min. Scale bar is 25 nm.

oleate ligand and oleylamine (Figure 2a). Monitoring the −COOH proton peak at 11.78 ppm with ^{1}H NMR of the chloro oleyl niobium(V) complex before and after aminolysis further supports our interpretation of the FTIR spectra. First, we inspect the niobium-to-oleic acid concentration series and find that the proton peak is absent in the 1-to-1 ratio case (Figure S5). This peak steadily reappears as the oleic acid content increases while the niobium content is fixed, indicating that the niobium complex is not completely coordinated with oleates. The NMR was measured in dry dimethyl sulfoxide-d_6 (DMSO-d_6) to collect a sharp −COOH proton peak, but during the formation of the chloro oleyl niobium(V) complex, the liberated chlorine interacts with the remaining free acidic protons in solution, decreasing the intensity of the acidic proton peak. After degassing the chloro oleyl niobium(V) complex at 120 °C, we observe an increase in the −COOH proton peak that we attribute to the removal of free chlorine from solution. When oleylamine is added to the chloro oleyl niobium(V), we observe the emergence of a N−H peak at 7.64 ppm indicative of amide formation caused by the aminolysis of niobium oleate (Figure 2b).[47] The proton from the amine that is removed during aminolysis forms OH^- and the metal oxo species is formed as all the amine is used in the reaction. The acidic proton from the remaining oleic acid reappears after the metal oxo species is formed as there is no further interaction with free Cl^- or oleylamine. It should be noted that this limited aminolysis occurs only after proper degassing to remove the hydrochloric acid that results from the niobium oleate formation. This is because excess hydrochloric acid would react with the amine as a Brønsted−Lowry acid and base pair, which is a competing reaction to the aminolysis for the niobium oxo cluster species. Thus, while degassing of the solution does not lead to further exchange toward a more complete niobium oleate, it is nevertheless critical for the subsequent limited aminolysis reaction (Figure S5).

After the limited aminolysis reaction, the mechanism progresses through three distinct steps (Figure 3): formation of niobium oxo clusters below 200 °C (Figure S6), condensation of niobium oxo clusters into amorphous niobium oxide seeds between 200 and 210 °C, and crystallization of amorphous seeds into niobium oxide nanorods. These stages are clearly revealed in Figure 3a,b through the evolution of the XRD patterns and Raman spectra as the reaction temperature increases. XRD reveals the gradual emergence of crystalline diffraction peaks and synthesis of a crystalline product at 220 °C. The Raman spectra of the intermediate products obtained at 200 and 210 °C exhibit a broad peak at 600 cm^{-1} characteristic of a mixture of NbO_6, NbO_7, and NbO_8 polyhedra in amorphous niobium oxide.[45] The transition from an amorphous material to an ordered structure occurring between 210 and 220 °C manifests as a sharpening and shift toward higher energies of the niobium−oxygen bridging stretches from 600 to 675 cm^{-1}. Interestingly, the Raman spectrum of the amorphous Nb_2O_5 product (200 °C) reveals that the broad peak at 600 cm^{-1} is accompanied by strong terminal niobium−oxygen double bond stretches at 800 cm^{-1}. Similar Raman spectra have been reported for amorphous niobium oxide composed of a chainlike network of niobium oxide polyhedra that was formed by the hydrolysis-driven condensation of polyoxoniobate clusters.[7,48] These observations suggest that the amorphous seeds formed by aminolysis of niobium oxo clusters are only partially condensed. The gradual decrease in intensity and broadening of the terminal niobium−oxygen double bond stretches, relative to the bridging niobium−oxygen band, between 200 and 210 °C indicate that the condensation of amorphous niobium oxide continues as the system approaches the crystallization temperature. STEM images corroborate this schema with low contrast pseudospherical particles at 200 °C followed by the formation of amorphous asymmetric nanoparticles at 210 °C that then grow into crystalline T-Nb_2O_5 nanorods at elevated temperatures.

One key benefit of this lower temperature aminolysis-based synthesis of T-Nb_2O_5 nanorods is their colloidal stability for the casting of functional thin films. In order to process the nanorods into switchable electrochromic thin films, we employed a strategy similar to that used on tungsten oxide nanorods to yield ligand-free colloidal dispersions that can be spin-coated as films on transparent conducting oxide FTO-coated glass.[5] Briefly, the as-synthesized nanorods are ligand-stripped in solution with a nitrosonium tetrafluoroborate procedure that leaves the surface positively charged and free of

DOI: 10.1021/acs.chemmater.9b04061
Chem. Mater. 2020, 32, 468−475

its native insulating layer. This electrostatically stabilized surface enables repulsion between nanorods to promote disordered packing and yield porous thin films. The procedure was discussed in detail in the previous paper[5] and is summarized in the Experimental Section. The step-by-step characterization of the process is included in the Supporting Information (Figure S7).

Unlike prior reports of crystalline niobium oxide electrochromism that extends from the visible regime to the near-infrared, these T-Nb_2O_5 nanorod films exhibit an electrochromic response that is predominantly in the infrared upon application of a reducing potential (Figure 4a). Cyclic

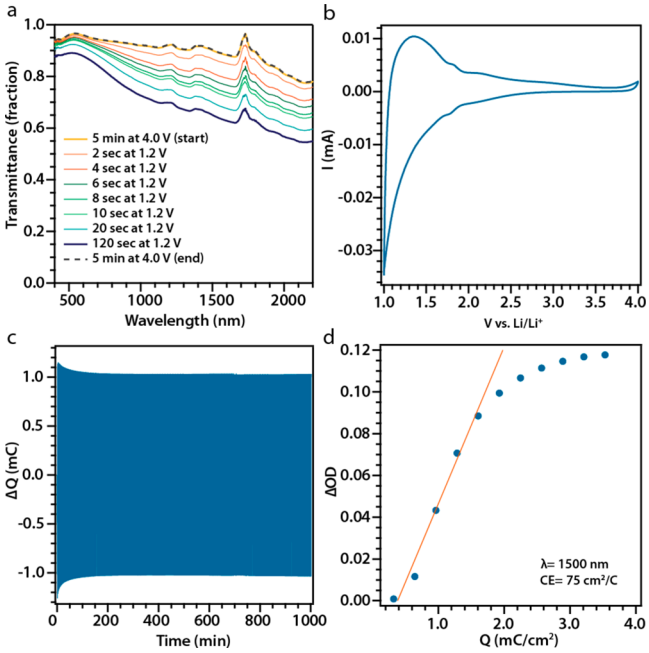

Figure 4. Electrochromic performance of T-Nb_2O_5 nanorod films. (a) Transmittance spectra of a nanorod film at 4.0 V ("clear" mode) and 1.2 V ("dark" mode) at different times. Dashed line corresponds to the second bleaching cycle. (b) Cyclic voltammetry of the same film at 1 mV/s scan rate. (c) Charge and discharge behavior of the same film by cycling the applied potential between 4.0 and 1.2 V 500 times (each potential step was applied for 1 min). (d) Coloration efficiency (CE = ΔOD/ΔQ) of the same film was determined by fitting the linear region of the plot with ΔOD measured at λ = 1500 nm. Blue circles are experimental data points, and the orange line is the fit result. See Figure S10 for CE at λ = 500 nm.

voltammetry performed to identify the cathodic and anodic peaks shows an anodic peak and a cathodic peak at 1.82 and 1.78 V vs Li/Li^+, respectively (Figure 4b). Time dependent measurements of the electrochromic response shown in Figure 4a further demonstrate that the reversible coloration behavior is fast. The time to reach maximum contrast is on the order of 120 s for a typical test case electrolyte of 1 M LiTFSI in tetraglyme and decreases to 60 s and increases to 200 s for 3 and 0.1 M electrolyte concentrations, respectively, suggesting that coloration kinetics are limited primarily by the conductivity of the electrolyte (Figure S8). This observation of fast kinetics is consistent with prior reports of fast Li^+ intercalation within crystalline niobium oxide materials, be it nanostructured or not.[49] Finally, these electrochromic films can be cyclically bleached and colored up to 500 cycles stably with no significant signs of degradation (Figure 4c). The coloration efficiency at 1500 nm was determined as 75 cm^2/C (Figure 4d, see Figure S9 and the Supporting Information for experimental details) and compares favorably to prior coloration efficiency reports for Nb_2O_5 films, which are between 24 and 47 cm^2/C.[31] The observed cathodic and anodic potentials, fast kinetics, and cyclic stability are consistent with previously studied solid-state processed (sputter-coated or chemical vapor deposited) thin films of T-Nb_2O_5.[17,50] Fast switching kinetics have been attributed to fast Li^+ diffusion along the [001] direction in the orthorhombic lattice and therefore anticipated in the nanorod films where the [001] direction is the predominant crystal direction. For cyclic stability specifically, we assume that prior solution processed sol–gel niobium oxide films[19] are not durable, likely due to poor crystallinity or the presence of impurity phases, since cyclic performance tests are not discussed in prior studies. The solution-processed nanorods here exhibit cyclic stability comparable to sputter processed films, which is attributed to the high crystal quality and phase purity afforded by colloidal nanocrystal synthesis.

One key finding in this study is the anomalous spectroelectrochemical response of these nanorod films. Unlike prior reports on niobium oxide electrochromism where amorphous systems demonstrate a predominantly visible response and crystalline systems demonstrate a response across the visible and infrared regime, these T-Nb_2O_5 nanorod films show an electrochromic response predominantly in the near-infrared. Prior studies have suggested that the visible response is dependent on polaronic coloration intrinsic to the Nb_2O_5 system while the infrared response may arise from Drude reflection upon electrochemical reduction of the system.[16] To shed light on the origins of coloration, we performed a series of experiments to test (i) the role of Li^+ intercalation and reduction of Nb^{5+}, (ii) the emergence of Drude reflection or a localized surface plasmon resonance upon charging, and (iii) the possible change in accessible polaronic modes due to dimensional constraint. First, films of T-Nb_2O_5 nanorods were tested with a different electrolyte of nonintercalating TBATFSI in tetraglyme. As shown in Figure S11, no electrochromic response was observed.

This establishes the noncapacitive nature of both the visible electrochromism and the infrared electrochromism and their dependence on Li^+ intercalation. Next, air-free XPS was conducted on as-prepared niobium oxide films and Li^+ intercalated films to determine the oxidation state of niobium in the film post electrochemical charging. Shown in Figure 5a,c, the niobium formal oxidation state begins as +5 and becomes a mix of +5 and +4 upon reduction and Li^+ intercalation.[51] This establishes eq 1 as still the primary mechanism for coloration for the nanorods. We also estimated the extent of Li^+ intercalation to be 4.2% of the total stoichiometry by quantifying the ratio of Nb^{4+} and Nb^{5+} and assuming that only intercalated Li^+ compensates for this difference in charge. Next, we investigate the second possibility that an increase in free electrons in the system contributes a metallic Drude reflection in the infrared regime or a localized surface plasmon resonance in the case of a nanocrystal film. To test these hypotheses, we deconvoluted the transmission spectra into their constitutive reflection and absorption components. Figure S12 shows that when the niobium oxide nanorod films are charged, there is no observable reflection component. This suggest that both the visible modulation and near-infrared modulation are a result of a polaronic response in

DOI: 10.1021/acs.chemmater.9b04061
Chem. Mater. 2020, 32, 468–475

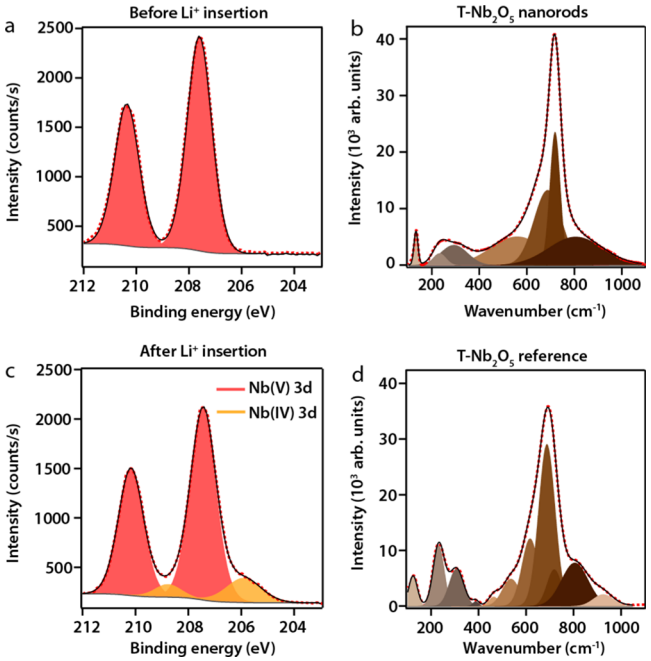

Figure 5. Nature of T-Nb_2O_5 infrared electrochromism. (a, c) T-Nb_2O_5 nanorod films before and after charging (Li^+ intercalation). XPS calibration was done using the Nb_2O_5 O 1s peak at 530.7 eV. (b, d) Deconvolution of the as-synthesized T-Nb_2O_5 nanorods and reference T-Nb_2O_5 Raman spectra. Details of the peak-fitting procedure and results are included in Table S1.

Nb_2O_5 and are not a result of a metallic Drude reflection. By changing the dielectric constant of the electrolyte surrounding the charged film, there is also no observable change in the optical spectra thus ruling out the emergence of a localized surface plasmon upon charging (Figure S13). Finally, it is only by deconvoluting the Raman spectrum of the T-Nb_2O_5 nanorods and comparing it to the bulk counterpart that we obtain a plausible explanation for this anomalous behavior (Figure 5b,d). From the comparison, we see that there are significant differences between the Raman spectra of bulk and nanorod T-Nb_2O_5.[52,53] Prior studies addressing the changes in Raman modes for T-Nb_2O_5 pre- and postlithiation have shown shifts, but not systematic broadening of Raman modes or disappearance of contributions to the absorption spectra.[54] Those results suggest that the Raman spectra we measured of the pristine nanorods and bulk powder should be qualitatively representative of the phonon modes responsible for coloration postlithiation. Comparing the two samples, we observe general broadening of various phonon modes and the disappearance of one of the high-energy longitudinal optical phonon modes at 925 cm^{-1} for the T-Nb_2O_5 nanorods. These changes in Raman active phonon modes may be caused by anisotropic nanostructuring since the nanorod width is comparable to the size of a single T-Nb_2O_5 unit cell (a = 0.62 nm, b = 2.9 nm, and c = 0.39 nm) in the a direction and smaller in the b direction, while the nanorod length is larger than the unit cell in the c direction. More importantly, as phonon modes, such as high-energy longitudinal optical phonon modes (925 cm^{-1}), are key enablers of polaronic absorption in Nb_2O_5, the disappearance of this high-energy mode might explain the low visible optical response of this material compared to its bulk counterpart. This analysis further suggests that the visible and infrared absorptions are polaronic responses that are intricately associated with the a–b and c axis directions in the crystal structure, respectively. More broadly, this observation motivates investigations of synthetic methods that can enable independent tuning of crystallite dimensions to select for specific polaronic electrochromic responses by controlling the presence or absence of specific phonon modes and, in turn, polaronic modes.

CONCLUSION

In summary, we demonstrate the colloidal synthesis of T-Nb_2O_5 nanorods through the aminolysis of a chloro oleyl niobium(V) complex to yield colloidally stable nanorods that can be further processed into electrochromic thin films. We show that the synthesis proceeds through the initial formation of niobium oxo clusters via aminolysis of chloro oleyl niobium(V) species, condensation to form small amorphous Nb_2O_5 seeds, and final crystallization and growth at 240 °C to yield high aspect ratio nanorods. These materials, when tested as solution deposited films, exhibit properties comparable to sputter-coated Nb_2O_5 thin films with the exception of electrochromic coloration that is predominantly in the near-infrared. Further investigation of this phenomenon reveals that both the visible and infrared colorations for T-Nb_2O_5 are triggered by polaronic responses that are associated strongly with specific crystalline directions. The synthesis of an anisotropic nanocrystal, that has a width approximately equal to or smaller than the a and b dimensions of one unit cell, seems to affect the accessibility of phonon modes that support polaronic absorption in the visible range upon charging. Further studies to elucidate the specific link between various phonon modes and coloration behavior in niobium oxide systems are in preparation. More broadly, this study demonstrates how dimensional control achieved through colloidal nanocrystal synthesis can be exploited to tune the properties of traditional electrochromic materials such as niobium oxide as well as to open a new opportunity to study the physics that underlie the optical responses of these materials.

ASSOCIATED CONTENT

Supporting Information

The Supporting Information is available free of charge at https://pubs.acs.org/doi/10.1021/acs.chemmater.9b04061.

Details of synthesis aliquots (FTIR, NMR, Raman), ligand-stripped nanorods (FTIR, ζ potential, SEM), spectroelectrochemistry (GITT, coloration efficiency, effect of electrolyte concentration, nonintercalating electrolyte measurement, reflection measurement, effect of dielectric environment), and Raman fitting (PDF)

AUTHOR INFORMATION

Corresponding Author

*E-mail: milliron@che.utexas.edu.

ORCID

Camila A. Saez Cabezas: 0000-0002-8734-0096
Manuel N. Dominguez: 0000-0002-9606-9234
Susanne Linn Skjærvø: 0000-0002-7753-5674
Delia J. Milliron: 0000-0002-8737-451X

Author Contributions

‖G.K.O. and C.A.S.C. contributed equally to this work.

DOI: 10.1021/acs.chemmater.9b04061
Chem. Mater. 2020, 32, 468–475

Notes

The authors declare the following competing financial interest(s): D.J.M. has a financial interest in Heliotrope Technologies, a company pursuing commercialization of electrochromic devices.

■ ACKNOWLEDGMENTS

We thank Clayton J. Dahlman, Ankit Agrawal, Hsin-Che Lu, and Yang Wang for helpful discussions and suggestions. This research was supported by the National Science Foundation (NSF MRSEC DMR-1720595; C.A.S.C. and M.N.D.), CBMM, and the Welch Foundation (F-1848). This research was also supported by the NSF Graduate Research Fellowship DGE 1106400 (to G.K.O) and DGE 1610403 (to M.N.D).

■ REFERENCES

(1) Kim, J. W.; Augustyn, V.; Dunn, B. The Effect of Crystallinity on the Rapid Pseudocapacitive Response of Nb_2O_5. *Adv. Energy Mater.* **2012**, *2* (1), 141−148.
(2) Augustyn, V.; Come, J.; Lowe, M. A.; Kim, J. W.; Taberna, P.-L.; Tolbert, S. H.; Abruña, H. D.; Simon, P.; Dunn, B. High-Rate Electrochemical Energy Storage through Li^+ Intercalation Pseudocapacitance. *Nat. Mater.* **2013**, *12* (6), 518−522.
(3) Fu, Z.-W. W.; Kong, J. J.; Qin, Q. Z. Electrochemical and Electrochromic Properties of Niobium Oxide Thin Films Fabricated by Pulsed Laser Deposition. *J. Electrochem. Soc.* **1999**, *146* (10), 3914−3918.
(4) Llordés, A.; Garcia, G.; Gazquez, J.; Milliron, D. J. Tunable near-Infrared and Visible-Light Transmittance in Nanocrystal-in-Glass Composites. *Nature* **2013**, *500* (7462), 323−326.
(5) Heo, S.; Kim, J.; Ong, G. K.; Milliron, D. J. Template-Free Mesoporous Electrochromic Films on Flexible Substrates from Tungsten Oxide Nanorods. *Nano Lett.* **2017**, *17* (9), 5756−5761.
(6) Kim, J.; Ong, G. K.; Wang, Y.; LeBlanc, G.; Williams, T. E.; Mattox, T. M.; Helms, B. A.; Milliron, D. J. Nanocomposite Architecture for Rapid, Spectrally-Selective Electrochromic Modulation of Solar Transmittance. *Nano Lett.* **2015**, *15* (8), 5574−5579.
(7) Llordés, A.; Wang, Y.; Fernandez-Martinez, A.; Xiao, P.; Lee, T.; Poulain, A.; Zandi, O.; Saez Cabezas, C. A.; Henkelman, G.; Milliron, D. J. Linear Topology in Amorphous Metal Oxide Electrochromic Networks Obtained via Low-Temperature Solution Processing. *Nat. Mater.* **2016**, *15* (12), 1267−1273.
(8) Le Viet, A.; Jose, R.; Reddy, M. V.; Chowdari, B. V. R.; Ramakrishna, S. Nb_2O_5 Photoelectrodes for Dye-Sensitized Solar Cells: Choice of the Polymorph. *J. Phys. Chem. C* **2010**, *114*, 21795−21800.
(9) Chen, S. G.; Chappel, S.; Diamant, Y.; Zaban, A. Preparation of Nb_2O_5 Coated TiO_2 Nanoporous Electrodes and Their Application in Dye-Sensitized Solar Cells. *Chem. Mater.* **2001**, *13* (12), 4629−4634.
(10) Ou, J. Z.; Rani, R. A.; Ham, M. H.; Field, M. R.; Zhang, Y.; Zheng, H.; Reece, P.; Zhuiykov, S.; Sriram, S.; Bhaskaran, M.; et al. Elevated Temperature Anodized Nb_2O_5: A Photoanode Material with Exceptionally Large Photoconversion Efficiencies. *ACS Nano* **2012**, *6* (5), 4045−4053.
(11) Kadir, R. A.; Rani, R. A.; Zoolfakar, A. S.; Ou, J. Z.; Shafiei, M.; Wlodarski, W.; Kalantar-Zadeh, K. Nb_2O_5 Schottky Based Ethanol Vapour Sensors: Effect of Metallic Catalysts. *Sens. Actuators, B* **2014**, *202*, 74−82.
(12) Dai, Z.; Dai, H.; Zhou, Y.; Liu, D.; Duan, G.; Cai, W.; Li, Y. Monodispersed Nb_2O_5 Microspheres: Facile Synthesis, Air/Water Interfacial Self-Assembly, Nb_2O_5-Based Composite Films, and Their Selective NO_2 Sensing. *Adv. Mater. Interfaces* **2015**, *2*, 1500167.
(13) Ab Kadir, R.; Rani, R. A.; Alsaif, M. M. Y. A.; Ou, J. Z.; Wlodarski, W.; O'Mullane, A. P.; Kalantar-Zadeh, K. Optical Gas Sensing Properties of Nanoporous Nb_2O_5 Films. *ACS Appl. Mater. Interfaces* **2015**, *7*, 4751−4758.
(14) Rani, R. A.; Zoolfakar, A. S.; O'Mullane, A. P.; Austin, M. W.; Kalantar-Zadeh, K. Thin Films and Nanostructures of Niobium Pentoxide: Fundamental Properties, Synthesis Methods and Applications. *J. Mater. Chem. A* **2014**, *2* (38), 15683−15703.
(15) Schäfer, H.; Gruehn, R.; Schulte, F. The Modifications of Niobium Pentoxide. *Angew. Chem., Int. Ed. Engl.* **1966**, *5* (1), 40−52.
(16) Schmitt, M.; Aegerter, M. A. Electrochromic Properties of Pure and Doped Nb_2O_5 Coatings and Devices. *Electrochim. Acta* **2001**, *46* (13−14), 2105−2111.
(17) Yoshimura, K.; Miki, T.; Tanemura, S. Electrochromic Properties of Niobium Oxide Thin Films Prepared by DC Magnetron Sputtering. *J. Electrochem. Soc.* **1997**, *144* (9), 2982.
(18) Reichman, B.; Bard, A. J. Electrochromism at Niobium Pentoxide Electrodes in Aqueous and Acetonitrile Solutions. *J. Electrochem. Soc.* **1980**, *127* (1), 241.
(19) Ohtani, B.; Iwai, K.; Nishimoto, S.; Inui, T. Electrochromism of Niobium Oxide Thin Films Prepared by the Sol-Gel Process. *J. Electrochem. Soc.* **1994**, *141* (9), 2439.
(20) Naito, K.; Matsui, T. Review on Phase Equilibria and Defect Structures in the Niobium-Oxygen System. *Solid State Ionics* **1984**, *12*, 125−134.
(21) Naito, K.; Kamegashira, N.; Sasaki, N. Phase Equilibria in the System between NbO_2 and Nb_2O_5 at High Temperatures. *J. Solid State Chem.* **1980**, *35* (3), 305−311.
(22) Ali, R. F.; Nazemi, A. H.; Gates, B. D. Surfactant Controlled Growth of Niobium Oxide Nanorods. *Cryst. Growth Des.* **2017**, *17* (9), 4637−4646.
(23) Luo, H.; Wei, M.; Wei, K. Synthesis of Nb_2O_5 Nanorods by a Soft Chemical Process. *J. Nanomater.* **2009**, *2009*, 758353.
(24) He, J.; Hu, Y.; Wang, Z.; Lu, W.; Yang, S.; Wu, G.; Wang, Y.; Wang, S.; Gu, H.; Wang, J. Hydrothermal Growth and Optical Properties of Nb_2O_5 Nanorod Arrays. *J. Mater. Chem. C* **2014**, *2* (38), 8185−8190.
(25) Deng, B.; Lei, T.; Zhu, W.; Xiao, L.; Liu, J. In-Plane Assembled Orthorhombic Nb_2O_5 Nanorod Films with High-Rate Li^+ Intercalation for High-Performance Flexible Li-Ion Capacitors. *Adv. Funct. Mater.* **2018**, *28* (1), 1704330.
(26) Li, B.; Gu, M.; Nie, Z.; Wei, X.; Wang, C.; Sprenkle, V.; Wang, W. Nanorod Niobium Oxide as Powerful Catalysts for an All Vanadium Redox Flow Battery. *Nano Lett.* **2014**, *14* (1), 158−165.
(27) Zhao, W.; Zhao, W.; Zhu, G.; Lin, T.; Xu, F.; Huang, F. Black Nb_2O_5 Nanorods with Improved Solar Absorption and Enhanced Photocatalytic Activity. *Dalt. Trans.* **2016**, *45* (9), 3888−3894.
(28) Yu, J.; Cheung, K. W.; Yan, W. H.; Li, Y. X.; Ho, D. High-Sensitivity Low-Power Tungsten Doped Niobium Oxide Nanorods Sensor for Nitrogen Dioxide Air Pollution Monitoring. *Sens. Actuators, B* **2017**, *238*, 204−213.
(29) Shi, C.; Xiang, K.; Zhu, Y.; Zhou, W.; Chen, X.; Chen, H. Box-Implanted Nb_2O_5 Nanorods as Superior Anode Materials in Lithium Ion Batteries. *Ceram. Int.* **2017**, *43* (15), 12388−12395.
(30) Fu, Z.-W.; Kong, J.-J.; Qin, Q.-Z. Electrochemical and Electrochromic Properties of Niobium Oxide Thin Films Fabricated by Pulsed Laser Deposition. *J. Electrochem. Soc.* **1999**, *146* (10), 3914.
(31) Yao, D. D.; Rani, R. A.; O'Mullane, A. P.; Kalantar-zadeh, K.; Ou, J. Z. High Performance Electrochromic Devices Based on Anodized Nanoporous Nb_2O_5. *J. Phys. Chem. C* **2014**, *118* (1), 476−481.
(32) Ohtani, B.; Iwai, K.; Nishimoto, S. I.; Inui, T. Electrochromism of Niobium Oxide Thin Films Prepared by the Sol-Gel Process. *J. Electrochem. Soc.* **1994**, *141* (9), 2439−2442.
(33) Gilroy, K. D.; Ruditskiy, A.; Peng, H.-C.; Qin, D.; Xia, Y. Bimetallic Nanocrystals: Syntheses, Properties, and Applications. *Chem. Rev.* **2016**, *116* (18), 10414−10472.
(34) Wang, D.; Kang, Y.; Ye, X.; Murray, C. B. Mineralizer-Assisted Shape-Control of Rare Earth Oxide Nanoplates. *Chem. Mater.* **2014**, *26* (22), 6328−6332.
(35) Dinh, C.-T.; Nguyen, T.-D.; Kleitz, F.; Do, T.-O. Shape-Controlled Synthesis of Highly Crystalline Titania Nanocrystals. *ACS Nano* **2009**, *3* (11), 3737−3743.

DOI: 10.1021/acs.chemmater.9b04061
Chem. Mater. 2020, 32, 468−475

(36) Gordon, T. R.; Paik, T.; Klein, D. R.; Naik, G. V.; Caglayan, H.; Boltasseva, A.; Murray, C. B. Shape-Dependent Plasmonic Response and Directed Self-Assembly in a New Semiconductor Building Block, Indium-Doped Cadmium Oxide (ICO). *Nano Lett.* **2013**, *13* (6), 2857−2863.
(37) Shieh, F.; Saunders, A. E.; Korgel, B. A. *J. Phys. Chem. B* **2005**, *109*, 8538−8542.
(38) Jana, S.; Rioux, R. M. Seeded Growth Induced Amorphous to Crystalline Transformation of Niobium Oxide Nanostructures. *Nanoscale* **2012**, *4* (5), 1782.
(39) Dong, A.; Ye, X.; Chen, J.; Kang, Y.; Gordon, T.; Kikkawa, J. M.; Murray, C. B. A Generalized Ligand-Exchange Strategy Enabling Sequential Surface Functionalization of Colloidal Nanocrystals. *J. Am. Chem. Soc.* **2011**, *133* (4), 998−1006.
(40) Llordes, A.; Hammack, A. T.; Buonsanti, R.; Tangirala, R.; Aloni, S.; Helms, B. A.; Milliron, D. J. Polyoxometalates and Colloidal Nanocrystals as Building Blocks for Metal Oxide Nanocomposite Films. *J. Mater. Chem.* **2011**, *21*, 11631−11638.
(41) Villa, E. M.; Ohlin, C. A.; Balogh, E.; Anderson, T. M.; Nyman, M. D.; Casey, W. H. Reaction Dynamics of the Decaniobate Ion $[H_xNb_{10}O_{28}]^{(6-x)-}$ in Water. *Angew. Chem., Int. Ed.* **2008**, *47*, 4844−4846.
(42) Yu, W. W.; Falkner, J. C.; Yavuz, C. T.; Colvin, V. L. Synthesis of Monodisperse Iron Oxide Nanocrystals by Thermal Decomposition of Iron Carboxylate Salts. *Chem. Commun.* **2004**, *356* (20), 2306.
(43) Kim, B. H.; Lee, N.; Kim, H.; An, K.; Park, Y. Il; Choi, Y.; Shin, K.; Lee, Y.; Kwon, S. G.; Na, H. B.; et al. Large-Scale Synthesis of Uniform and Extremely Small-Sized Iron Oxide Nanoparticles for High-Resolution T_1 Magnetic Resonance Imaging Contrast Agents. *J. Am. Chem. Soc.* **2011**, *133* (32), 12624−12631.
(44) Park, J.; An, K.; Hwang, Y.; Park, J.-G.; Noh, H.-J.; Kim, J.-Y.; Park, J.-H.; Hwang, N.-M.; Hyeon, T. Ultra-Large-Scale Syntheses of Monodisperse Nanocrystals. *Nat. Mater.* **2004**, *3* (12), 891−895.
(45) Jehng, J. M.; Wachs, I. E. Structural Chemistry and Raman Spectra of Niobium Oxides. *Chem. Mater.* **1991**, *3* (1), 100−107.
(46) Marchetti, F.; Pampaloni, G.; Zacchini, S. Chemistry of Niobium and Tantalum Halides, MX_5, with Haloacetic Acids and Their Related Anhydrides: Anhydride C-H Bond Activation Promoted by MF_5. *Polyhedron* **2008**, *27* (8), 1969−1976.
(47) Soderberg, T. *Organic Chemistry with a Biological Emphasis Vol. I*; Chemistry Publications 1; University of Minnesota Morris: rev. 2019. https://digitalcommons.morris.umn.edu/chem_facpubs/1.
(48) Jehng, J.-M.; Wachs, I. E. Niobium Oxide Solution Chemistry. *J. Raman Spectrosc.* **1991**, *22* (2), 83−89.
(49) Griffith, K. J.; Forse, A. C.; Griffin, J. M.; Grey, C. P. High-Rate Intercalation without Nanostructuring in Metastable Nb_2O_5 Bronze Phases. *J. Am. Chem. Soc.* **2016**, *138* (28), 8888−8899.
(50) Maruyama, T.; Kanagawa, T. Electrochromic Properties of Niobium Oxide Thin Films Prepared by Chemical Vapor Deposition. *J. Electrochem. Soc.* **1994**, *141* (10), 2868.
(51) Kuznetsov, M. V.; Razinkin, A. S.; Shalaeva, E. V. Photoelectron Spectroscopy and Diffraction of Surface Nanoscale NbO/Nb(110) Structures. *J. Struct. Chem.* **2009**, *50* (3), 514−521.
(52) Brayner, R.; Bozon-Verduraz, F. Niobium Pentoxide Prepared by Soft Chemical Routes: Morphology, Structure, Defects and Quantum Size Effect. *Phys. Chem. Chem. Phys.* **2003**, *5*, 1457−1466.
(53) McConnell, A. A.; Aderson, J. S.; Rao, C. N. R. Raman Spectra of Niobium Oxides. *Spectrochim. Acta Part A Mol. Spectrosc.* **1976**, *32* (5), 1067−1076.
(54) Chen, D.; Wang, J.-H.; Chou, T.-F.; Zhao, B.; El-Sayed, M. A.; Liu, M. Unraveling the Nature of Anomalously Fast Energy Storage in T-Nb_2O_5. *J. Am. Chem. Soc.* **2017**, *139* (20), 7071−7081.

DOI: 10.1021/acs.chemmater.9b04061
Chem. Mater. 2020, 32, 468−475